Dalton Transactions

PAPER

Chiral rhodium complexes covalently anchored on carbon nanotubes for enantioselective hydrogenation†

C. C. Gheorghiu,[a] B. F. Machado,[b,c] C. Salinas-Martínez de Lecea,[a] M. Gouygou,*[b,c] M. C. Román-Martínez*[a] and P. Serp[b,c]

Chiral rhodium hybrid nanocatalysts have been prepared by covalent anchorage of pyrrolidine-based diphosphine ligands onto functionalized CNTs. This work constitutes the first attempt at covalent anchoring of homogeneous chiral catalysts on CNTs. The catalysts, prepared with two different chiral phosphines, were characterized by ICP, XPS, N_2 adsorption and TEM, and have been tested in the asymmetric hydrogenation of two different substrates: methyl 2-acetamidoacrylate and α-acetamidocinnamic acid. The hybrid nanocatalysts have shown to be active and enantioselective in the hydrogenation of α-acetamidocinnamic acid. A good recyclability of the catalysts with low leaching and without loss of activity and enantioselectivity was observed.

Introduction

Carbon materials have proved to be suitable supports for heterogeneous catalysis, due to their high versatility in terms of textural/surface properties as well as morphology, together with chemical inertness under many conditions, thermal stability and mechanical resistance.[1,2] In particular, nanostructured carbon materials are preferred because of a potential confinement effect.[3,4] Among them, carbon nanotubes (CNTs) showed interesting structures and properties, leading therefore to promising applications as catalyst supports.[5,6] They are usually preferred to other classical carbon materials, like activated carbon, because they are mesoporous. Thus, the accessibility to the supported active phase is better and the reaction is not negatively affected by mass transfer limitations. In some cases, the superior properties of supported CNT catalysts have been attributed to the existence of a strong metal–support interaction.[7,8]

When enantioselective catalysts are immobilized on solid supports, the resulting catalysts combine the advantages of both, homogeneous (selectivity, tunability and homogeneous sites) and heterogeneous (recovery and separation) catalysts.[9–11] For enantioselective hydrogenation, many of the most successful diphosphine ligands have been anchored onto inorganic platforms, leading to comparable performance in terms of enantioselectivity and efficiency than their homogeneous counterparts.[12–17] If some attempts to immobilize hydrogenation catalysts on conventional carbons have been reported,[18,19] the use of CNTs as supports for the immobilization of a homogeneous catalyst has surprisingly not been extensively developed, particularly if we consider the rich chemistry dealing with CNT surface functionalization.[20–31] Among the different possible immobilization strategies[9] the most common is the covalent one, and to the best of our knowledge only a few studies have dealt with the covalent anchoring of a homogeneous catalyst on CNTs[22–31] and none of chiral rhodium-based catalysts. The most common method for anchoring a ligand on carbon materials consists in the formation of an amide bond between the oxidized carbon material and amino-tagged ligands. In this context, pyrrolidine-based diphosphine ligands (PPM family, PPM is 2S,4S-4-diphenylphosphino-2-diphenylphosphinomethylpyrrolidine), which are efficient ligands in rhodium(I) catalyzed asymmetric hydrogenation of olefins,[32–34] are good candidates for a covalent anchoring.[35–38]

The present work reports on the preparation of chiral rhodium hybrid nanocatalysts by covalent anchorage of PPM-based ligands onto functionalized CNTs (Scheme 1), and their characterization and application in asymmetric catalysis.

[a]Department of Inorganic Chemistry and Materials Institute, University of Alicante, ctra San Vicente del Raspeig s/n., 03690 Alicante, Spain. E-mail: mcroman@ua.es
[b]CNRS, LCC (Laboratoire de Chimie de Coordination, Composante ENSIACET), 4 allée Emile Monso, BP 44362, F-31030 Toulouse Cedex 4, France.
E-mail: maryse.gouygou@lcc-toulouse.fr
[c]Université de Toulouse, UPS, INPT, F-31077 Toulouse Cedex 4, France
†Electronic supplementary information (ESI) available. See DOI: 10.1039/c3dt53301h

Experimental

All commercially available reagents were used as received. The anhydrous solvents were obtained from a Solvent Purification
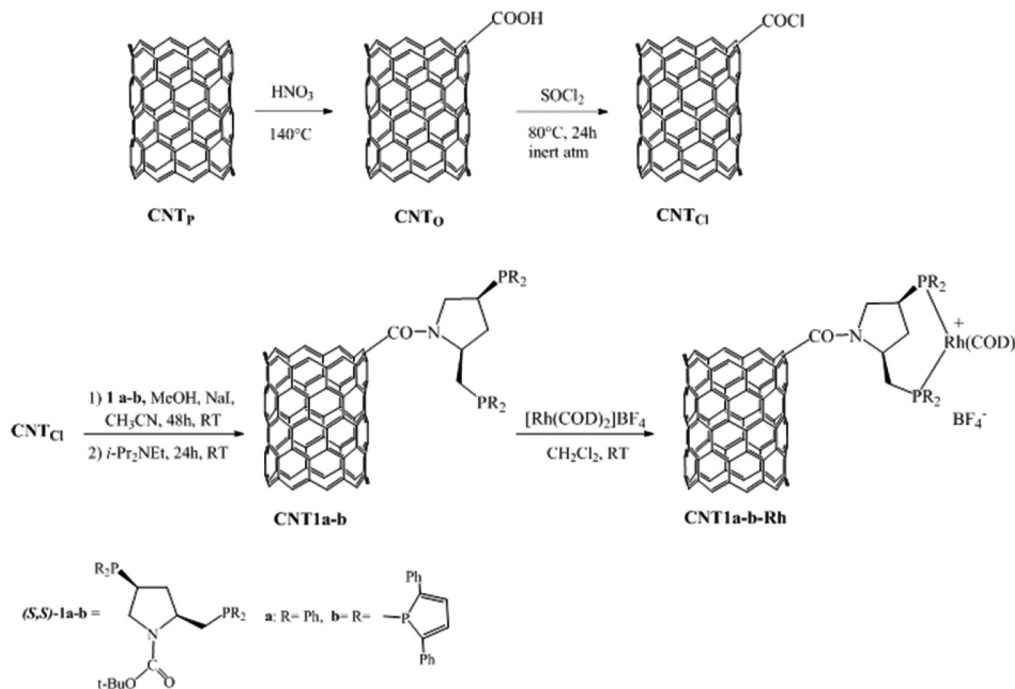
Scheme 1 Covalent grafting of chiral Rh complex on CNT surface.

System (Innovative Technologies) or distillated with the appropriate drying agents and they were degassed prior to use. The inert atmosphere reactions were run under nitrogen or argon using standard Schlenk techniques.

Preparation of functionalized carbon nanotubes, CNT_{Cl}

The carbon nanotubes used in this work are multi-walled carbon nanotubes, prepared by the catalytic-CVD method.[39] This sample was named **CNT**. It has been subjected to a purification treatment to remove the Fe/Al_2O_3 catalyst used in the synthesis process. Such a treatment is as follows: the sample was put in contact with a 50% vol. H_2SO_4–H_2O mixture (100 mL g_{CNT}^{-1}) for 3.5 h under reflux and stirring. Then, the solid was separated by filtration, thoroughly washed with distilled water and dried at 120 °C for two days. The purified sample was named CNT_P.

The CNT_P were oxidized by treatment with a nitric acid solution (65 wt%), 100 mL solution per gram of carbon, at 140 °C, under stirring, for 4 hours. Afterwards, the mixture was left to cool down and filtered, followed by washing with cold distilled water, until a stable pH of the rinsing water was reached. The sample was then dried at 120 °C for two days. The oxidized carbon nanotubes were named CNT_O.

The surface carboxylic groups produced by the oxidation treatment were further transformed into acyl chloride groups by reaction with $SOCl_2$ according to the following procedure: under an inert atmosphere (N_2), sample CNT_O was mixed with $SOCl_2$ (approximately 40 mL per gram of the sample), and the mixture was kept at reflux temperature (80 °C) and constant stirring for 24 hours. Then, it was cooled down and the liquid was removed under vacuum. The solid was vacuum dried

overnight at room temperature and stored under an inert atmosphere to avoid hydrolysis of the acyl chloride functionalities. After this treatment, the support was named CNT_{Cl}.

Preparation of chiral diphosphines

N-(tert-butoxycarbonyl)-(2S,4S)-4-diphenylphosphino-2-[(diphenylphosphino)-methyl]-pyrrolidine, (S,S)-1a. A solution of N-(tert-butoxycarbonyl)-4-hydroxy-L-prolinol di-p-toluenesulfonate[34] (0.85 g, 1.6 mmol) in 10 mL of dry THF was added under an inert atmosphere to 8.53 mL (4.26 mmol) of a solution of potassium diphenylphosphide, Ph_2PK, 0.5 M in THF. The mixture was stirred at room temperature for 35 hours under an inert atmosphere. Then, the solution was treated with methanol to remove the anion excess, filtered and concentrated under vacuum. The yellow viscous residue was crystallized from 9 mL of anhydrous ethanol and the solid was washed with a CH_2Cl_2–pentane mixture (50 : 50) and then purified by alumina column chromatography. ^{31}P NMR ($CDCl_3$): δ −22.57 (s, 1P), −14.94 (s, 1P).[40] ^{1}H NMR ($CDCl_3$): δ 1.43 (s, 9H, CH_3), 1.69–2.31 (m, 3H), 2.76–3.26 (m, 3H), 3.68–4.00 (m, 2H), 7.35–7.58 (m, 20H, Ph); see ESI.1.† ^{13}C NMR ($CDCl_3$): δ 28.59 (s, $(CH_3)_3C$), 35.82 (m, CH–P), 38.02 (m, CH_2–P), 50.32 (m, CH_2), 56.20 (m, CH), 79.90 (s, $(CH_3)_3C$), 128.43–128.99 (m, C_{Ph}), 132.67–133.37 (m, C_{Ph}), 136.94 (m, C_{ipso}), 137.63 (m, C_{ipso}), 153.99 (s, C=O); see ESI.2.†

N-(tert-butoxycarbonyl)-(2S,4S)-4-[2′,5′-diphenylphospholyl]-2-[(2′,5′-diphenyl-phospholyl)methyl]-pyrrolidine, (S,S)-1b. The synthesis of diphosphine **1b** was accomplished by the same procedure as described above for **1a** using 2,5-diphenylphospholyl lithium[41] instead of PPh_2PK. ^{31}P NMR ($CDCl_3$): δ −13.30 (s, 1P), −7.69 (s, 1P). ^{1}H NMR ($CDCl_3$): δ 1.50 (s, 9H, CH_3),

1.60–2.25 (m, 3H), 3.40–3.60 (m, 3H), 4.16 (bs, 1H), 4.39 (bs, 1H), 7.18–7.65 (m, 20H, Ph); see ESI.3.† ^{13}C NMR (CDCl$_3$): δ 28.44 (s, (CH$_3$)$_3$C), 37.88 (s, CH–P), 55.86 (s, CH$_2$–P), 58.92 (s, CH$_2$), 67.43 (s, CH), 80.66 (s, CH$_3$)$_3$C), 126–136–44 (m, C$_{Ar}$), 151.51 (s, C=O); see ESI.4.†

Preparation of chiral diphosphine supported on CNTs, CNT1a-b

0.45 g of sample **CNT$_{Cl}$** was added to a solution containing the **1a** diphosphine ligand (0.768 g, 1.38 mmol), MeOH (0.5 mL) and anhydrous NaI (0.19 g, 1.3 mmol) in CH$_3$CN (6 mL). The mixture was stirred for 2 days at room temperature. Then, *N,N*-diisopropylethylamine (DIPEA) (0.44 mL, 2.5 mmol) was added at 0 °C, and the mixture was stirred for 24 hours at room temperature. Finally, 9 mL of degassed HCl solution (10 wt% aq.) were added to the solution to neutralize the excess of base. The filtration procedure for the isolation of **CNT1a-b** was performed under an inert atmosphere, using a filter funnel with drip-tip and one on side-arm, frit porosity 25–50 μm, and with a 47 mm diameter 0.2 μm pore size nuclepore hydrophilic PC (polycarbonate) filter membrane. Afterwards, the solid was washed with a saturated aqueous solution of NaHCO$_3$ (10 mL), ethanol (2 × 10 mL) and diethyl ether (4 × 10 mL). The solid was dried and stored under argon.

The preparation of **CNT1b** was accomplished following the same procedure as described above for **CNT1a**, using 0.072 g of **CNT$_{Cl}$** and 0.072 g (0.110 mmol) of **1b**.

Preparation of chiral Rh-complex supported on CNTs, CNT1a-b-Rh. 200 mg of **CNT1a** were impregnated with a solution of anhydrous dichloromethane (7 mL) containing 15 mg of [Rh-(COD)$_2$]BF$_4$ (0.037 mmol). These amounts correspond to 2 wt% rhodium on the solid catalyst. The mixture was stirred at room temperature for 24 h under an inert atmosphere, and then, the catalyst was filtered (under an inert atmosphere, *via* cannula) and washed first with a mixture of CH$_2$Cl$_2$–pentane (50 : 50) (3 × 8 mL) and then with CH$_2$Cl$_2$ (5 × 5 mL). Subsequently, the catalyst was dried under an inert atmosphere at room temperature for 24 h.

The synthesis of **CNT1b-Rh** was performed in the same way using 50 mg of **CNT1b** and 4 mg of [Rh(COD)$_2$]BF$_4$ complex (0.01 mmol).

Characterization techniques

TEM analysis was used to get information about the morphology of the investigated samples. It was performed with a JEOL JEM-2010 equipment.

Samples **CNT**, **CNT$_P$** and **CNT$_O$** were analyzed by thermogravimetry (TG) with the purpose of studying their reactivity in air and to determine the ash amount (related to impurities). For the experiments, carried out in a thermobalance SDT TA Instruments 2960, the samples were heated, at 10 °C min^{-1}, up to 1000 °C in synthetic air flow (100 cm^3 min^{-1}).

The textural properties of the original and oxidized carbon nanotubes were analyzed by gas adsorption: N$_2$ at −196 °C and CO$_2$ at 0 °C, using the automatic volumetric apparatus Auto-sorb-6B. The samples were previously degassed at 250 °C for 4 h. The textural properties of the samples (BET surface area, pore volumes of different size range, pore size distributions)

were determined as described in the literature.[40] Briefly, the total micropore volume ($V_{μt}$) was determined by applying the Dubinin–Radushkevich (DR) equation to the N$_2$ adsorption data. A similar calculation on the CO$_2$ adsorption data gives the volume of the narrower micropores ($V_{nμ}$). The volume of supermicropores ($V_{sμ}$) was determined by the subtraction $V_{μt} − V_{nμ}$. Finally, mesopore volumes (V_{meso}) were calculated as difference between the amount of nitrogen adsorbed at 0.97 and 0.2 P/P^0 expressed as a liquid.[40,41]

The study of the surface chemistry was carried out by Temperature Programmed Desorption (TPD), using a thermobalance SDT TA Instruments 2960 coupled to a mass spectrometer Blazers MSC 200 Thermostar. Approximately 10 mg of the sample were heated, at 20 °C min^{-1}, up to 1100 °C in 20 cm^3 min^{-1} He flow.

Samples **CNT$_O$** and **CNT$_{Cl}$** were analysed by FT-IR spectroscopy using a Nicolet 380 device.

Supports and catalysts were analysed by XPS using the equipment VG-Microtech Mutilab 3000 with MgKα (1253.6 eV) radiation. Pressure for measurements was 5 × 10^{-10} mbar. C1s transition was adjusted to 284.6 eV.

NMR spectra were recorded at 25 °C on a Bruker Avance 300 or on a DPX300 spectrometer.

Enantiomeric excess (ee) was determined by chiral GC using the equipment Agilent Technologies 7820 A with a flame ionization detector (FID) and the capillary column CP-1Chirasil-L-Val (25 m × 250 μm × 0.12 μm) with decane as an internal standard.

General procedure for the asymmetric hydrogenation

To a stainless steel Parr reactor was added a mixture of 80 mg (0.560 mmol) of substrate, 30 mg of **CNT1a-b-Rh** in 7 mL anhydrous methanol. We used 30 mg of the hybrid catalyst that correspond to 0.32 mg Rh or 0.18 mg Rh when using the catalyst **CNT1a-Rh** or **CNT1b-Rh**, respectively. The reactor was pressurized with H$_2$ to 5.5 bar at room temperature and the reaction mixture was stirred (1100 rpm) for an appropriate time. After reaction, the hydrogen pressure was carefully released and the catalyst was recovered *via* filtration under a nitrogen atmosphere and then washed with fresh solvent. Afterwards it was used in a new catalytic run under the same conditions. The conversion and ee values of products were determined by GC chromatography after the acids had been transformed into the corresponding esters for compound **3b**.[42]

The homogeneous catalytic experiments were performed with [Rh(COD)PPM]BF$_4$ (3.5 mg, 4.7 μmol) prepared *in situ* by adding 2.3 mg (5 μmol) of (*S,S*)-PPM ligand to a methanol solution containing 1.9 mg (4.7 μmol) of [Rh(COD)$_2$]BF$_4$. After 1 hour of stirring at room temperature, 175 mg (1.2 mmol) of **2a** substrate were added and the resulting solution was directly transferred into a stainless steel autoclave and the reaction was started under the same experimental conditions as those described above.

Results and discussion

Synthesis of chiral Rh-complexes supported on CNTs

For anchoring diphosphine ligands, the CNTs were firstly modified to generate surface acyl groups.[43] A two-step
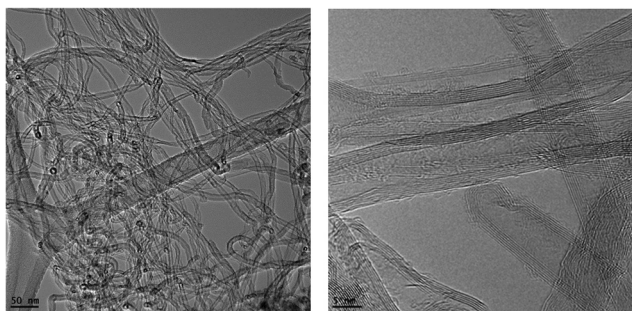
Fig. 1 TEM micrographs of sample CNT$_O$.

Fig. 2 Thermogravimetric profiles obtained for samples CNT, CNT$_P$ and CNT$_O$.

procedure gave rise to the functionalized carbon nanotubes **CNT$_{Cl}$** (Scheme 1). In order to perform the coupling reaction under mild conditions, because of the sensitivity of diphosphine compounds, we have chosen the procedure reported by Nazih *et al.*,[44] which allows the direct conversion of an N-protected amine into an amide species. This procedure involved the synthesis of diphosphine ligands tailored for immobilization. The amino-tagged chiral diphosphines **1a–b** were synthesized according to slightly modified reported procedures.[32,34] Then, the reaction of **CNT$_{Cl}$** with ligands **1a–b** was conducted at room temperature in CH$_3$CN in the presence of MeOH and NaI (Scheme 1). This one-pot procedure implies the *in situ* (i) cleavage of the Boc group (*tert*-butoxycarbonyl group) with HI generated from the reaction of MeOH with the acyl group in the presence of NaI and (ii) amide bond formation in the presence of a base. After treatment, filtration and purification, the resulting CNT tethered diphosphines, **CNT1a-b**, were analysed by XPS (*vide supra*). In the last step, the immobilized diphosphines, **CNT1a-b**, were reacted with the rhodium (ı) complex [Rh(COD)$_2$]BF$_4$ in CH$_2$Cl$_2$ at room temperature to produce the hybrid catalysts **CNT1a-b-Rh** (Scheme 1), which were characterized by ICP and XPS (*vide supra*).

Characterization of carbon nanotubes

Fig. 1 shows TEM micrographs of **CNT$_O$**. These images show that **CNT$_O$** present few compartments (bamboo like structure) and that they are characterized by outer and inner diameters of 20–25 nm and 7–10 nm, respectively. For comparison TEM

micrographs of pristine CNT and CNT$_P$ are shown in ESI.5.† No significant difference in terms of morphology was noticed for the three samples, except for some CNT tip opening in sample **CNT$_O$** (see below).

Samples **CNT**, **CNT$_P$** and **CNT$_O$**, were analysed by thermogravimetry (TG). Fig. 2 shows the obtained thermograms.

The reactivity in air of samples **CNT** and **CNT$_P$** is similar; the differences observed for the oxidized sample **CNT$_O$** are due to the decomposition of surface oxygen groups.[45] Regarding the ash content, these data show that the original **CNT** sample contains 6.35 wt%, that is reduced to 2.82 wt% after the purification treatment and to 0.92 wt% after the HNO$_3$ treatment (sample **CNT$_O$**). Fig. 3a shows the N$_2$ adsorption isotherms obtained for samples **CNT** and **CNT$_O$**.

These isotherms are of type IIb according to the subdivision of the IUPAC classification presented by Rouquerol *et al.*,[46] and are indicative of capillary condensation. It is considered that the porosity of multi-walled CNTs consists mainly of the inner hollow cores and pores formed by bundles of nanotubes.[47–49] The presence of hysteresis can be related to the presence of pores with both ends open.[50,51] Sample **CNT$_O$** shows an increase of the adsorption capacity compared to the original sample that reveals CNT tip opening upon such a
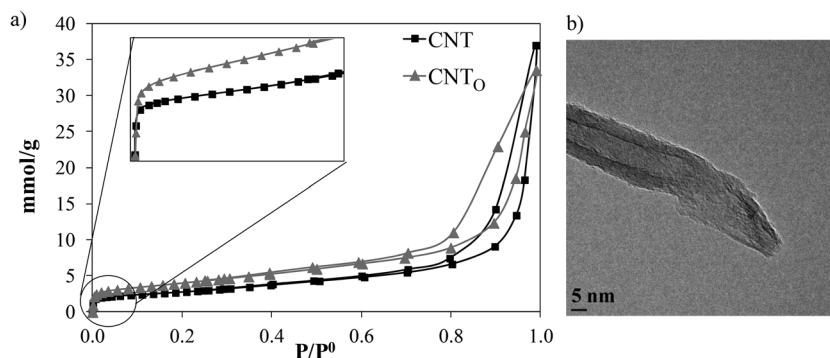
Fig. 3 (a) N$_2$ adsorption isotherms at −196 °C of samples **CNT** and **CNT$_O$** and (b) TEM micrograph of an opened CNT.

Table 1 Textural properties of the original and oxidized CNTs

Sample	S_{BET} [m^2 g^{-1}]	$V_{\mu t}$ [cm^3 g^{-1}]	$V_{n\mu}$ [cm^3 g^{-1}]	$V_{s\mu}$ [cm^3 g^{-1}]	V_{meso} [cm^3 g^{-1}]
CNT	222	0.09	0.041	0.047	0.54
CNT$_O$	323	0.13	0.070	0.061	0.73

S_{BET}, BET surface area; $V_{\mu t}$, total micropore volume; $V_{n\mu}$, narrow micropore volume; $V_{s\mu}$, supermicropore volume; V_{meso}, mesopore volume (calculated between 0.2 and 0.97 P/P^0).

Table 2 Quantification of TPD profiles: CO and CO$_2$ evolved, oxygen weight percentage, and amount of carboxylic acid type groups (calculated by deconvolution of the CO$_2$ desorption profile)

Sample	CO [μmol g^{-1}]	CO$_2$ [μmol g^{-1}]	O [%]	Carboxylic acid [μmol g^{-1}]
CNT	847	100	1.7	0
CNT$_P$	697	150	1.6	0
CNT$_O$	1742	1076	6.2	425
CNT$_{Cl}$	533	870	3.6	126

treatment (Fig. 3b).[52] Table 1 includes the surface area and porosity parameters determined from the adsorption data.

The data show that the purification and oxidation treatments produce an increase of the BET surface area and of the pore volumes in the whole range of porosity. Fig. 4 shows the CO and CO$_2$ evolution profiles obtained during TPD experiments for samples **CNT**, **CNT$_P$**, **CNT$_O$** and **CNT$_{Cl}$**.

It can be observed that the purification treatment produces no significant changes in the surface chemistry of the supports (only a slight decrease of groups which decompose as CO). However, the oxidation treatment with nitric acid produces an important amount of surface oxygen groups and further treatment with SOCl$_2$ leads to a significant reduction in the evolution of both CO and CO$_2$.

The quantification of the TPD profiles as the amount of CO and CO$_2$ evolved (in μmol g^{-1}) and the calculated oxygen weight percentage are shown in Table 2. The amount of carboxylic acid groups, necessary to create the –COCl functionalities for the covalent bond with the diphosphine ligands, has been determined by deconvolution of the CO$_2$ evolution profile, considering that this kind of groups decompose between 130 °C and 350 °C.[53,54] After the acylation treatment, the amount of carboxylic acid groups (first peak) is considerably reduced (Table 2), indicating that the transformation of the carboxylic acid groups occur.

The FT-IR spectra for samples **CNT$_O$** and **CNT$_{Cl}$** (Fig. 5) show the peak at 1567 cm^{-1}, assigned to C=C stretching, which originates from the inherent structure of CNTs and also the peaks at 1720 and 1200 cm^{-1} arising from C=O and C–O stretching, respectively, indicating the existence of carboxylic

Fig. 5 FT-IR spectra of **CNT$_O$** and **CNT$_{Cl}$** samples.

groups, visible in both samples. The spectrum of sample **CNT$_{Cl}$** additionally exhibits a shoulder at 1760 cm^{-1} corresponding to the acetyl chloride. A decrease in the intensity of the peak at 3450 cm^{-1} corresponding to O–H stretch from carboxylic acid groups in sample **CNT$_{Cl}$** is noticeable. This observation, together with the variation of the band at 1200 cm^{-1}, is indicative of the transformation of carboxylic acid groups. The appearance of a characteristic peak at 592 cm^{-1}, corresponding to C–Cl stretch in acetyl chloride, confirms the formation of acyl chloride groups. Signal assignments were performed according to literature data.[55–57]
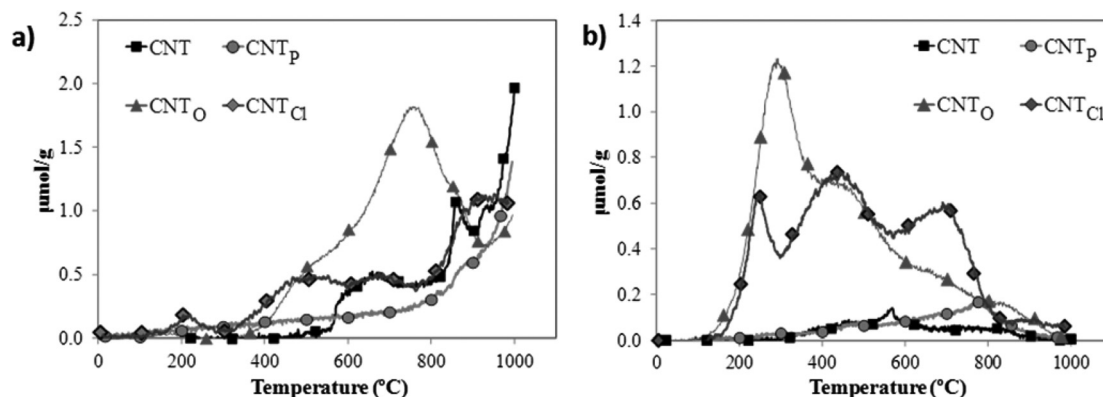
Fig. 4 TPD desorption profiles for the original, purified and functionalized CNTs: (a) CO and (b) CO$_2$ evolutions.

These data confirmed the effective transformation of carboxylic into acyl chloride groups. However, in agreement with the TPD data, not all the COOH groups were converted, as signals due to carboxyl groups are still present in the spectrum of sample **CNT$_{Cl}$**. This might be due to partial hydrolysis of the surface acetyl chloride functionalities during air exposure.

Characterization of the tethered chiral diphosphine ligands

Samples **CNT1a** and **CNT1b** have been analysed by XPS (see spectra in ESI.6 and ESI.7†) and the obtained results are summarized in Table 3. For comparison purposes, data for the (2S,4S)-4-diphenylphosphino-2-[(diphenylphosphino)methyl]-pyrrolidine ligand, **PPM**, have been also included. It can be observed that the binding energy of P 2p in the carbon tethered diphosphines **CNT1a** and **CNT1b** is higher than in the free PPM ligand. This can be attributed to a modification of the P electronic state due to the interaction with the support surface.[58,59] The binding energy found for N 1s (around 400 eV) is characteristic of nitrogen in amine form.[60,61] The P/N ratio is close to the theoretical one (P/N = 2).

Characterization of the hybrid catalysts, CNT1a-Rh and CNT1b-Rh

The amount of rhodium determined by ICP-OES in the **CNT1a-Rh** fresh catalysts is 1.05 wt%, corresponding to 145 μmol of complex per gram of sample, while for catalyst **CNT1b-Rh** the amount is 0.6 wt% corresponding to 83 μmol of complex per gram of sample. XPS data are shown in Table 3. It can be observed that the binding energies of P 2p and N 1s almost do not change upon rhodium coordination. The binding energy of Rh 3d$_{5/2}$ corresponds to rhodium(I), indicating that the electronic state of rhodium in the complex is not modified upon heterogenisation. The Rh/P ratio, higher than the theoretical value (0.5), can be interpreted considering the presence of a certain amount of rhodium not coordinated to the phosphine ligands.

Enantioselective hydrogenation. The catalytic performances of the hybrid catalysts **CNT1a-b-Rh** were explored in the asymmetric hydrogenation of 2-methylacetamidoacrylate (**2a**) and α-acetamidocinnamic acid (**2b**) (Scheme 2).

In the first set of experiments, the hydrogenation reaction of 2-methylacetamidoacrylate (**2a**) was investigated at room temperature under 5.5 bar of dihydrogen (Table 4). The results were compared with those obtained from two reference

Table 3 XPS data of the carbon-tethered diphosphine and hybrid catalysts

Sample	Binding energy [eV]				Atomic ratio	
	P 2p	N 1s	C 1s	Rh 3d$_{5/2}$	P/N	Rh/P
PPM	130.8	399.0	284.7	—	2.3	—
CNT1a	133.0	399.8	284.6	—	2.7	—
CNT1a-Rh	132.9	400.3	284.5	308.5	1.5	0.7
CNT1b	132.4	400.0	284.5	—	1.3	—
CNT1b-Rh	132.2	400.1	284.6	309.1	0.9	1.1

Scheme 2 Enantioselective hydrogenation of methyl 2-acetamidoacrylate and α-acetamidocinnamic acid.

Table 4 Enantioselective hydrogenation of methyl 2-acetamidoacrylate, **2a**[a]

Entry	Catalysts	S/C	Run	Time (h)	Conversion[b] (%)	ee[b]
1	**[Rh(COD)$_2$]BF$_4$**	140	1	42	90	/
2	**(S,S)-PPM-Rh**	250	1	2	20	7 (R)
3	**CNT1a-Rh**	200	1	20	100	11 (R)
4	**CNT1a-Rh**		2	3	100	12 (R)
5	**CNT1a-Rh**		3	3	100	10 (R)
6	**CNT1a-Rh**		3[c]	3	70	/
7	**CNT1b-Rh**	300	1	4	100	16 (R)
8	**CNT1b-Rh**		2	4	100	15 (R)

[a] Reaction conditions: 5.5 bar H$_2$, at RT in MeOH. [b] Determined by chiral GC using a CP-1 Chirasil-L-Val column with decane as an internal standard. [c] Catalytic run using liquid phase.

experiments. As the first reference, we used [Rh(COD)$_2$]BF$_4$ as a catalyst without the diphosphine ligand. As can be observed in Table 4 (entry 1), the conversion obtained after 42 h of reaction (90%) shows the low activity of this catalyst. The second reference was the homogeneous catalyst **(S,S)-PPM-Rh**, prepared in situ from the **(S,S)-PPM** ligand and the [Rh(COD)$_2$]BF$_4$ precursor. This catalyst shows also low activity and selectivity under reaction conditions (Table 4, entry 2). The stability of the hybrid catalysts under reaction conditions (24 h) was evaluated performing a run without the presence of the substrate. In this case, no leaching was observed. The hybrid catalysts **CNT1a-b-Rh** proved to be active but moderately enantioselective for the hydrogenation of substrate **2a** (Table 4, entries 3–8). The moderate increase in selectivity observed compared to the homogeneous catalyst is probably the consequence of the acylation of the secondary amino group of the PPM ligand as already observed.[33,35]

The recyclability of hybrid **CNT1a-b-Rh** catalysts was evaluated in the hydrogenation of **2a**. After the first run, the **CNT1a-Rh** was recovered from the reaction mixture by filtration, washed with MeOH to remove traces of the previous mixture and engaged in a new catalytic run. A complete conversion of the substrate was obtained with the same enantioselectivity (Table 4, entry 4). Furthermore, we observed that the **CNT1a-Rh** catalyst becomes more active after having been used; for comparison the conversion was only 25% after 3 h with the fresh **CNT1a-Rh**. Interestingly, **CNT1a-Rh** still exhibited a high catalytic activity after 3 consecutive cycles without loss of enantioselectivity (Table 4, entry 5). At this stage, the liquid phase was engaged in another catalytic reaction after the addition of a fresh substrate. The conversion of the substrate

was 70% but no enantioselectivity could be measured (Table 4, entry 6). Similarly, **CNT1b-Rh** catalyst can be reused without loss of activity and enantioselectivity in two consecutive runs (Table 4, entries 7 and 8).

Encouraging results in terms of enantioselectivity were obtained in the hydrogenation of α-acetamidocinnamic acid, **2b** (Table 5). Indeed, the hybrid catalysts **CNT1a-b-Rh** are able to perform the hydrogenation reaction with good conversions (71–75%) producing enantiomeric excess in the range 54–63%. Compared to homogeneous catalytic systems reported in the literature (entries 1 and 2),[33] **CNT1a-b-Rh** proved to be more enantioselective but slightly less active.

Characterization of used catalysts. The amount of Rh remaining on the support after their use in several catalytic runs of 2-methyl-acetamidoacrylate hydrogenation was analysed by ICP (Table 6). The results showed that leaching is relatively low (less than 15%).

XPS analysis of the spent catalysts gives the following binding energies: Rh $3d_{5/2}$ 310 eV, P 2p 133 eV, N 1s 400 eV and C 1s 284.5 eV. These data suggest that the electronic state of the anchored complex has not been modified. However, the P/N and Rh/P atomic ratios are lower than in the fresh catalysts (0.30 and 0.42, respectively), meaning that some alteration of the complex structure has taken place.

The hybrid catalyst **CNT1a-Rh** was also analysed by TEM after 3 runs of 2-methyl acetamidoacrylate hydrogenation. Fig. 6 shows some of the micrographs obtained, where the presence of small metallic nanoparticles can be observed (size between 1 and 3 nm). It is expected that the same will happen after use in the hydrogenation of α-acetamidocinnamic acid, because reaction conditions are similar. The observation of Rh particles is surprising because Rh(0) was not detected by XPS, and also because the spent catalysts are still enantioselective. This means either that only a small part of the rhodium complex has been reduced (likely, the species not coordinated to
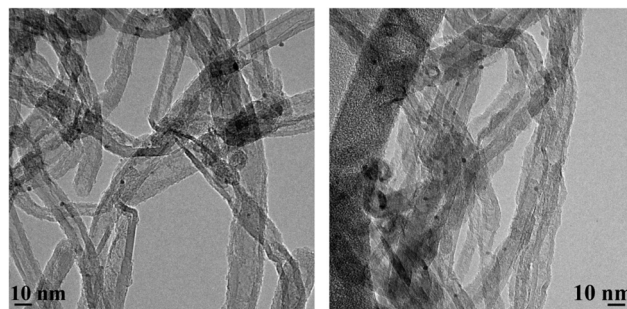

Fig. 6 TEM micrographs of the spent catalyst **CNT1a-Rh** (3 catalytic runs).

the tethered phosphines) and this small amount of Rh(0) is not detected by XPS, or that the Rh complex decomposition takes place under the electron beam of the TEM. Such a decomposition could be favoured with the spent catalyst since the complex has been altered, being less robust. The possible formation of low amounts of Rh(0) could explain the higher catalytic activity of the spent catalyst.[24] The fact that the ee are not significantly affected upon recycling could come from the fact that the R(0) nanoparticles are stabilized by the chiral ligand.[62] More analyses and experiments are needed to confirm this hypothesis.

Conclusions

Chiral rhodium complexes have been successfully grafted on CNTs for the first time. The grafting strategy consists of the synthesis and tether of the diphosphine ligands PPM on CNTs, followed by the reaction with a Rh precursor. The grafted complexes are active in the hydrogenation of methyl 2-acetamidoacrylate, with a modest enantioselectivity, and are fully reusable. Leaching was low and the ee did not decrease upon consecutive runs. The hybrid catalysts showed a very good activity for the hydrogenation of α-acetamidocinnamic acid and a better enantioselectivity than the homogeneous counterpart. Thus, this work opens prospects for the development of hybrid enantioselective catalysts on carbon nanostructures.

Acknowledgements

References

1 P. Serp, in *Comprehensive Inorganic Chemistry II*, ed. J. Reedijk and K. Poeppelmeier, Elsevier, Amsterdam, 2nd edn, 2013, pp. 323–369.

Table 5 Asymmetric hydrogenation of α-acetamidocinnamic acid, **2b**[a]

Entry	Catalysts	S/C	Time (h)	Conversion[b] (%)	ee[b]
1	**(S,S)-PPM-Rh**[c]	100	20	100	6 (S)
2	**(S,S)-BPPM-Rh**[c]	100	20	100	30 (R)
3	**CNT1a-Rh**	200	24	75	63 (R)
4	**CNT1b-Rh**	200	24	71	54 (R)

[a] Reaction conditions: 5.5 atm H_2, at RT in MeOH. [b] Determined by chiral GC using a CP-1 Chirasil-L-Val column with decane as an internal standard. [c] Data from the literature, see ref. 33.

Table 6 Amount of Rh remaining in catalyst **CNT1a-Rh** after several catalytic runs

Catalysts	Run	% Rh (mg) remaining in the catalyst	Leaching (%)
CNT1a-Rh	0	1.05 (0.347 mg)	/
CNT1a-Rh	1	0.94 (0.312 mg)	10
CNT1a-Rh	2	0.898 (0.297 mg)	4.6
CNT1a-Rh	3	0.897(0.296 mg)	0.2

2 F. Rodríguez-Reinoso and A. Sepulveda-Escribano, in *Carbon Materials for Catalysis*, ed. P. Serp and J. L. Figueiredo, John Wiley & Sons, Inc., 2009, pp. 131–155.

3 P. Serp and E. Castillejos, *ChemCatChem*, 2010, **2**, 41–47.

4 X. Pan and X. Bao, *Acc. Chem. Res.*, 2011, **44**, 553–562.

5 P. Serp, M. Corrias and P. Kalck, *Appl. Catal., A*, 2003, **253**, 337–358.

6 J. H. Bitter, *J. Mater. Chem.*, 2010, **20**, 7312–7321.

7 S. Karski, I. Witońska, J. Rogowski and J. Gołuchowska, *J. Mol. Catal. A: Chem.*, 2005, **240**, 155–163.

8 A. Chambers, T. Nemes, N. M. Rodriguez and R. T. K. Baker, *J. Phys. Chem. B*, 1998, **102**, 2251–2258.

9 Z. Wang, in *Handbook of Asymmetric Heterogeneous Catalysis*, ed. K. Ding and Y. Uozumi, Wiley-VCH Verlag GmbH & Co. KGaA, 2008, pp. 1–24.

10 H.-U. Blaser, B. Pugin and M. Studer, in *Chiral Catalyst Immobilization and Recycling*, ed. I. F. J. V. D. E. De Vos and P. A. Jacobs, Wiley-VCH Verlag GmbH, 2007, pp. 1–17.

11 G. J. Hutchings, *Annu. Rev. Mater. Res.*, 2005, **35**, 143–166.

12 D. J. Bayston and M. E. C. Polywka, in *Chiral Catalyst Immobilization and Recycling*, Wiley-VCH Verlag GmbH, 2007, pp. 211–234.

13 A. R. McDonald, C. Muller, D. Vogt, G. P. M. van Klink and G. van Koten, *Green Chem.*, 2008, **10**, 424–432.

14 D. J. Mihalcik and W. Lin, *Angew. Chem., Int. Ed.*, 2008, **47**, 6229–6232.

15 R. Sayah, M. Le Floch, E. Framery and V. Dufaud, *J. Mol. Catal. A: Chem.*, 2010, **315**, 51–59.

16 A. Börner, *Phosphorus ligands in asymmetric catalysis, Synthesis and Application*, Wiley-VCH Verlag GmbH, 2008.

17 A. Crosman and W. F. Hoelderich, *J. Catal.*, 2009, **265**, 229–237.

18 A. A. Tregubov, K. Q. Vuong, E. Luais, J. J. Gooding and B. A. Messerle, *J. Am. Chem. Soc.*, 2013, **135**, 16429–16437.

19 C. Freire and A. R. Silva, in *Carbon Materials for Catalysis*, ed. P. Serp and J. L. Figueiredo, John Wiley & Sons, Inc., 2009, pp. 267–307.

20 U. N. Maiti, W. J. Lee, J. M. Lee, Y. Oh, J. Y. Kim, J. E. Kim, J. Shim, T. H. Han and S. O. Kim, *Adv. Mater.*, 2014, **26**, 40–67.

21 N. Karousis, N. Tagmatarchis and D. Tasis, *Chem. Rev.*, 2010, **110**, 5366–5397.

22 L. Lemus-Yegres, I. Such-Basáñez, C. Salinas-Martínez de Lecea, P. Serp and M. C. Román-Martínez, *Carbon*, 2006, **44**, 605–608.

23 L. M. D. R. S. Martins, M. P. de Almeida, S. A. C. Carabineiro, J. L. Figueiredo and A. J. L. Pombeiro, *ChemCatChem*, 2013, **5**, 3847–3856.

24 C. C. Gheorghiu, C. Salinas-Martínez de Lecea and M. C. Román-Martínez, *ChemCatChem*, 2013, **5**, 1587–1597.

25 L. J. Lemus-Yegres, M. Pérez-Cadenas, M. C. Román-Martínez and C. Salinas-Martínez de Lecea, *Microporous Mesoporous Mater.*, 2011, **139**, 164–172.

26 L. J. Lemus-Yegres, M. C. Román-Martínez and C. Salinas-Martínez de Lecea, *J. Nanosci. Nanotechnol.*, 2009, **9**, 6034–6041.

27 Y. Zhang, H.-B. Zhang, G.-D. Lin, P. Chen, Y.-Z. Yuan and K. R. Tsai, *Appl. Catal., A*, 1999, **187**, 213–224.

28 C. Baleizão, B. Gigante, H. García and A. Corma, *Tetrahedron*, 2004, **60**, 10461–10468.

29 S. Banerjee and S. S. Wong, *J. Am. Chem. Soc.*, 2002, **124**, 8940–8948.

30 L. J. Lemus-Yegres, M. C. Román-Martínez, I. Such-Basáñez and C. Salinas-Martínez de Lecea, *Microporous Mesoporous Mater.*, 2008, **109**, 305–316.

31 M. Pérez-Cadenas, L. J. Lemus-Yegres, M. C. Román-Martínez and C. Salinas-Martínez de Lecea, *Appl. Catal., A*, 2011, **402**, 132–138.

32 I. Ojima, T. Kogure and N. Yoda, *J. Org. Chem.*, 1980, **45**, 4728–4739.

33 K. Achiwa, *J. Am. Chem. Soc.*, 1976, **98**, 8265–8266.

34 G. L. Baker, S. J. Fritschel, J. R. Stille and J. K. Stille, *J. Org. Chem.*, 1981, **46**, 2954–2960.

35 T. Malmström and C. Andersson, *J. Mol. Catal. A: Chem.*, 1999, **139**, 259–270.

36 C. Yang, Y. T. Wong, Z. Li, J. J. Krepinsky and G. Jia, *Organometallics*, 2001, **20**, 5220–5224.

37 I. Ojima, T. Kogure, N. Yoda, T. Suzuki, M. Yatabe and T. Tanaka, *J. Org. Chem.*, 1982, **47**, 1329–1334.

38 T. Malmstrom and C. Andersson, *Chem. Commun.*, 1996, 1135–1136.

39 A. Morançais, B. Caussat, Y. Kihn, P. Kalck, D. Plee, P. Gaillard, D. Bernard and P. Serp, *Carbon*, 2007, **45**, 624–635.

40 G. Parrinello and J. K. Stille, *J. Am. Chem. Soc.*, 1987, **109**, 7122–7127.

41 D. H. Nguyen, J. Bayardon, C. Salomon-Bertrand, S. Jugé, P. Kalck, J.-C. Daran, M. Urrutigoity and M. Gouygou, *Organometallics*, 2012, **31**, 857–869.

42 C. Pérez, S. Pérez, G. A. Fuentes and A. Corma, *J. Mol. Catal. A: Chem.*, 2003, **197**, 275–281.

43 L. Rodriguez-Perez, E. Teuma, A. Falqui, M. Gomez and P. Serp, *Chem. Commun.*, 2008, 4201–4203.

44 A. Nazih and D. Heissler, *Synthesis*, 2002, 0203–0206.

45 L. Van Thu, N. Cao Long, L. Quoc Trung, N. Trinh Tung, N. Duc Nghia and V. Minh Thanh, *Adv. Nat. Sci.: Nanosci. Nanotechnol.*, 2013, **4**, 035017.

46 F. Rouquerol, J. Rouquerol and K. Sing, in *Adsorption by Powders and Porous Solids*, ed. F. Rouquerol, J. Rouquerol and K. Sing, Academic Press, London, 1999, pp. 93–115.

47 F. Li, Y. Wang, D. Wang and F. Wei, *Carbon*, 2004, **42**, 2375–2383.

48 S. Inoue, N. Ichikuni, T. Suzuki, T. Uematsu and K. Kaneko, *J. Phys. Chem. B*, 1998, **102**, 4689–4692.

49 Q.-H. Yang, P.-X. Hou, S. Bai, M.-Z. Wang and H.-M. Cheng, *Chem. Phys. Lett.*, 2001, **345**, 18–24.

50 S. Lowell, J. Shields, M. Thomas and M. Thommes, in *Characterization of Porous Solids and Powders: Surface Area, Pore Size and Density*, ed. S. Lowell, J. Shields, M. Thomas and M. Thommes, Springer, Netherlands, 2004, vol. 16, ch. 3, pp. 11–14.

51 K. S. W. S. S. J. Gregg, *Adsorption, surface area, and porosity*, Academic Press, New York, 1982.

52 I. Gerber, M. Oubenali, R. Bacsa, J. Durand, A. Gonçalves, M. F. R. Pereira, F. Jolibois, L. Perrin, R. Poteau and P. Serp, *Chem.–Eur. J.*, 2011, **17**, 11467–11477.

53 J. L. Figueiredo, M. F. R. Pereira, M. M. A. Freitas and J. J. M. Órfão, *Carbon*, 1999, **37**, 1379–1389.

54 G. S. Szymański, Z. Karpiński, S. Biniak and A. Świàtkowski, *Carbon*, 2002, **40**, 2627–2639.

55 T. J. Bandosz, in *Carbon Materials for Catalysis*, ed. P. Serp and J. L. Figueiredo, John Wiley & Sons, Inc., 2009, pp. 45–92.

56 M. A. Atieh, O. Y. Bakather, B. Al-Tawbini, A. A. Bukhari, F. A. Abuilaiwi and M. B. Fettouhi, *Bioinorg. Chem. Appl.*, 2010, 603978.

57 C. Zhao, L. Ji, H. Liu, G. Hu, S. Zhang, M. Yang and Z. Yang, *J. Solid State Chem.*, 2004, **177**, 4394–4398.

58 E. Guillén, R. Rico, J. M. López-Romero, J. Bedia, J. M. Rosas, J. Rodríguez-Mirasol and T. Cordero, *Appl. Catal., A*, 2009, **368**, 113–120.

59 J. M. Rosas, J. Bedia, J. Rodríguez-Mirasol and T. Cordero, *Fuel*, 2009, **88**, 19–26.

60 S. R. Kelemen, M. Afeworki, M. L. Gorbaty, P. J. Kwiatek, M. S. Solum, J. Z. Hu and R. J. Pugmire, *Energy Fuels*, 2002, **16**, 1507–1515.

61 W. J. Gammon, O. Kraft, A. C. Reilly and B. C. Holloway, *Carbon*, 2003, **41**, 1917–1923.

62 S. Jansat, M. Gómez, K. Philippot, G. Muller, E. Guiu, C. Claver, S. Castillón and B. Chaudret, *J. Am. Chem. Soc.*, 2004, **126**, 1592–1593.